

# Characteristics and accumulation model of the late Quaternary shallow biogenic gas in the modern Changjiang delta area, eastern China

Xia Zhang<sup>1</sup> · Chun-Ming Lin<sup>1</sup>

Received: 20 June 2016 / Published online: 19 April 2017  
© The Author(s) 2017. This article is an open access publication

**Abstract** The Changjiang (Yangtze) is one of the largest rivers in the world. It formed a huge incised valley at its mouth during the Last Glacial Maximum; the incised-valley fill, approximately 80–110 m thick, supplies an important foundation for the generation of shallow biogenic-gas reservoirs. Two cores and 13 cone penetration tests were used to elaborate the characteristics, formation mechanism, and distribution of the shallow biogenic-gas reservoirs in the study area. The natural gas is mainly composed of CH<sub>4</sub> (generally >95%) with a  $\delta^{13}\text{C}_{\text{CH}_4}$  and  $\delta^{13}\text{C}_{\text{CO}_2}$  of  $-75.8$  to  $-67.7\text{‰}$  and  $-34.5$  to  $-6.6\text{‰}$ , respectively, and a  $\delta\text{D}_{\text{CH}_4}$  of  $-215$  to  $-185\text{‰}$ , indicating a biogenic origin by the carbon dioxide reduction pathway. Commercial biogenic gas occurs primarily in the sand bodies of fluvial-channel, floodplain, and paleo-estuary facies with a burial depth of 50–80 m. Gas sources as well as cap beds are gray to yellowish-gray mud of floodplain, paleo-estuary, and offshore shallow marine facies. The organic matter in gas sources is dominated by immature type III kerogen (gas prone). The difference in permeability (about 4–6 orders of magnitude) between cap beds and reservoirs makes the cap beds effectively prevent the upward escape of gas in the reservoirs. This formation mechanism is consistent with that for the shallow biogenic gas in the late Quaternary Qiantang River incised valley to the south. Therefore, this study should provide further insight into understanding the formation and distribution of shallow biogenic gas in other similar postglacial incised-valley systems.

**Keywords** Biogenic gas · Formation mechanism · Late Quaternary · Modern Changjiang delta · Eastern China

## 1 Introduction

Biogenic gas is of significant importance because it is clean energy and an abundant resource, accounting for ~20% of the conventional natural gas reserves in the world (Rice and Claypool 1981). Recently, researchers have drawn considerable attention to the shallow biogenic gas in the near-surface marine and coastal sediments such as bay or estuarine deposits and late Quaternary incised-valley fills (García-García et al. 2007; Xu et al. 2009; Lin et al. 2010; Zhang et al. 2013; Jones et al. 2014; Okay and Aydemir 2016), in terms of the shallow-burial depth ranging from several tens of meters to hundreds of meters and easy exploitation with low investment and high benefit. Commercial reservoirs of shallow biogenic gas have been widely found in the world, including the North Sea (Hegland 1997; Vielstädte et al. 2015), Ria de Vigo incised valley, Spain (García-Gil et al. 2002), western Gulf of Maine, USA (Rogers et al. 2006), and Lawrence Estuary, Canada (Pinet et al. 2008).

Shallow biogenic-gas reservoirs are principally distributed along the eastern and southern coasts of China, especially the Jiangsu–Zhejiang coastal plain area, where the postglacial Changjiang and Qiantang River incised valleys are located (Wang 1982; Zheng 1998; Lin et al. 2004; Liu et al. 2008; Li et al. 2010a; Zhang et al. 2013, 2014). Incised valleys generally have high preservation potential for their fill deposits (Dalrymple et al. 1994) and provide a fundamental and important background for the formation of the shallow biogenic-gas reservoirs therein, i.e., gas-source beds, cap beds, and sand

✉ Xia Zhang  
zhangxiananjing@163.com

<sup>1</sup> State Key Laboratory for Mineral Deposits Research, School of Earth Sciences and Engineering, Nanjing University, Nanjing 210023, Jiangsu, China

reservoirs can occur together in close geographic and stratigraphic proximity (Xu et al. 2009; Lin et al. 2004; Zhang et al. 2014). Considerable biogenic-gas accumulations with depth <120 m have been discovered and well documented in the late Quaternary Qiantang River incised valley with a predicted total gas amount of  $244.5 \times 10^9 \text{ m}^3$  (Lin et al. 2004, 2010; Zhang et al. 2013). Also, the produced gas was used as gas supply for local villages and factories (Li and Lin 2010). Nevertheless, there are relatively few examples in the scientific literature regarding the shallow biogenic gas in the Changjiang incised valley area after >60 years' research and development (cf. Wang 1982; Zheng 1998). Previous research indicates that shallow biogenic gas is mainly distributed in the northern margin of the modern Changjiang delta (i.e., the M area in Fig. 1a,  $\sim 2.5 \times 10^4 \text{ km}^2$ ; Wang 1982; Zheng 1998), and there are generally three sets of gas-bearing intervals with burial-depth ranges of 7–15, 25–35, and >50 m, respectively, involving prodelta–shallow marine, delta front, coastal plain, and floodplain facies (Zheng 1998).

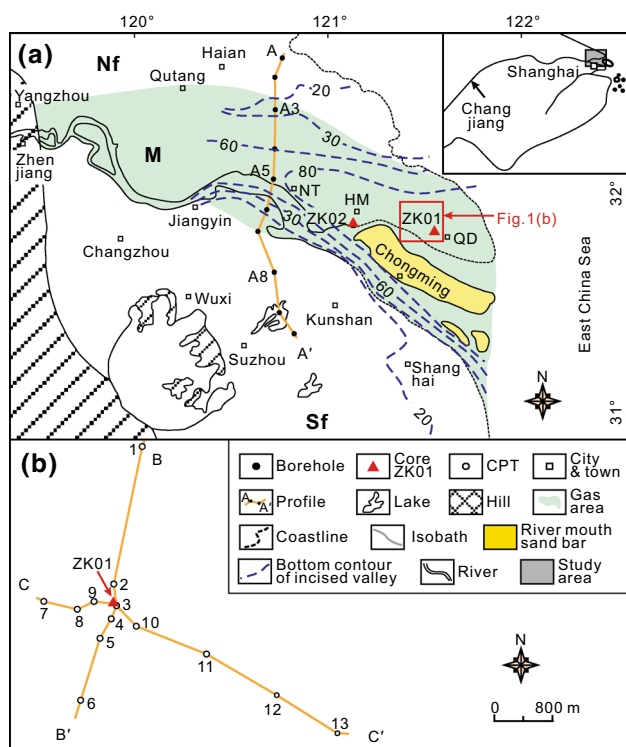


**Fig. 1** **a** Schematic map of the modern Changjiang (Yangtze River) delta showing the locations of cores ZK01 and ZK02, boreholes, cross section, and gas-bearing area, as well as the basal topography of the Changjiang incised valley during the Last Glacial Maximum (modified from Wang 1982; Zheng 1998; Li et al. 2002; Zhang et al. 2015). **b** Locations of core ZK01, cone penetration tests (CPTs), and transects in the Qidong area from the northern margin of the modern Changjiang delta (see location in Fig. 1a). *M* Main delta area, *Sf* Southern flank, *Nf* Northern flank, *QD* Qidong area, *HM* Haimen area, *NT* Nantong

Obviously, a poor understanding of the geological background, distribution, and formation of the shallow biogenic-gas reservoirs in the study area has seriously hampered the exploration and exploitation processes.

This paper is an extension of the previous work based primarily on the detailed observations and analyses of newly acquired cores ZK01 and ZK02, as well as 13 surrounding cone penetration tests (CPTs) in the Qidong and Haimen areas (Fig. 1), and the further correlation with more than 600 boreholes, most of which have been reported by Li et al. (2000, 2002) and Hori et al. (2002). The objective of this study is to discuss the conditions required for the formation of the shallow biogenic-gas reservoirs and to summarize the regularities of their distribution in the modern Changjiang delta area. This study will provide a useful insight into the exploration and exploitation of the shallow biogenic gas in similar incised-valley systems, more importantly for the modern Changjiang delta area, where there is dense population and tremendous economic development.

## 2 Geological setting

The Changjiang originating from the Qinghai–Tibet Plateau annually discharges water and sediment of  $924 \text{ km}^3$  and  $4.8 \times 10^{11} \text{ kg}$ , respectively (Milliman and Syvitski 1992), and provides the primary sediment source for the modern Changjiang delta. The present-day Changjiang delta is situated at a coastal subsidence zone, with the altitude generally <5 m above mean sea level (Stanley and Chen 1996). It is bounded by hills in the west (Fig. 1a) and slopes gently toward the east with  $\sim 250 \text{ km}$  in length from the apex around Zhenjiang–Yangzhou area to the modern river mouth. The modern Changjiang delta covers an area of  $\sim 5.2 \times 10^4 \text{ km}^2$ , with  $2.3 \times 10^4 \text{ km}^2$  subaerial and  $2.9 \times 10^4 \text{ km}^2$  subaqueous (Li et al. 2002). The former can be divided into three major units: the main delta body (M), and the southern (Sf) and northern (Nf) flanks (Li et al. 2002; Fig. 1a). The main body is characterized by the combination of distributary channels and three active river-mouth sand bars, which are elongated and extend south-eastward (Li et al. 2002). The subaqueous part of the delta can be classified into subtidal flats with water depths <5–10 m, delta front ranging from 5–10 to 15–30 m, and prodelta (water depth of >30 and <50 m).

## 3 Materials and methods

Cores ZK01 (112 m penetration depth, 0.1 m diameter) and ZK02 (128 m penetration depth, 0.1 m diameter) were taken from Qidong ( $31^\circ 50' 26.74'' \text{N}$ ,  $121^\circ 33' 24.08'' \text{E}$ ) and

Haimen (31°52′47.12″N, 121°09′30.69″E) areas where shallow gas is abundant, respectively, in 2014 by rotary drilling and with almost 100% recovery (see locations in Fig. 1a). In the laboratory, they were split, photographed, described, and subsampled. The grain size of 271 samples (0.5–1.0 m interval) was analyzed at 0.25 Φ spacing according to a standard method (cf. Zhou and Gao 2004), with grain-size parameters determined using the GRADISTAT software (Blott and Pye 2001). Eighty-three samples were collected for foraminifera analysis using the method described by Zhang et al. (2014) and Wang et al. (1988). The permeabilities of 16 samples were measured by falling-head permeability test apparatus (cf. Zhang et al. 2013). The total organic carbon (TOC) and chloroform bitumen contents of 41 samples were analyzed following the method of Stax and Stein (1993). Eight mud samples were obtained for pyrolysis analysis (cf. Zou et al. 2006). Four <sup>14</sup>C ages were determined on shells or organic sediments by using accelerator-based mass spectroscopy in the Beta Analytic Radiocarbon Dating Laboratory (Lab No. Beta) in Miami, USA, and calibrated using the Calib Rev 7.1 (beta) program (Reimer et al. 2013; Table 1). Two <sup>14</sup>C ages on marine shells were calibrated utilizing the Marine13 model with the Δ*R* value of 135 ± 42 to deal with the marine reservoir effect (cf. Yoneda et al. 2007; Wang et al. 2012).

In addition, 13 CPTs were taken around the ZK01 core (Fig. 1(b)), with the tested parameters being cone tip resistance (*q<sub>c</sub>*) and sleeve friction (*f<sub>s</sub>*), in order to explore the distribution pattern of shallow gas, i.e., potential sand reservoirs (cf. Moran et al. 1989; Li and Lin 2010). During exploration, almost every CPT inevitably encountered gas with an original gas pressure of ~0.5 MPa and a flame height reaching up to 2 m when the gas was ignited. In this study, a total of six gas samples were collected and analyzed for chemical composition, stable carbon isotope ratios of CH<sub>4</sub> and CO<sub>2</sub>, and stable hydrogen isotope ratios of CH<sub>4</sub> according to a standard method (cf. Ni et al. 2013). Furthermore, CPT-3 and the nearby ZK01 core were compared to calibrate the *q<sub>c</sub>* and *f<sub>s</sub>* curves allowing for distinguishing lithology, especially potential sandy

reservoirs (Fig. 1b). In general, *q<sub>c</sub>* and *f<sub>s</sub>* values increase as grain size increases (cf. Li and Lin 2010; Lin et al. 2015). Therefore, the *q<sub>c</sub>* and *f<sub>s</sub>* curves of sand and silt sediments show high values and large separation of curves, and the *q<sub>c</sub>* curve lies generally to the left of *f<sub>s</sub>* curve (cf. Li and Lin 2010; Lin et al. 2015).

### 4 Stratigraphic architecture

More than 600 cores were drilled in the present-day Changjiang delta area in the last five decades, laying a solid foundation for understanding the stratigraphic architecture of the coastal depositional system (Li et al. 2002; Hori et al. 2001; Wang et al. 2012). There are at least three stages for the formation of the Quaternary Changjiang incised-valley fills (Hori et al. 2002; Li and Wang 1998; Li et al. 2006; Figs. 1a, 2). Most of the incised-valley fills generated during the preceding two stages are missing resulted from the following strong down-cutting erosion and in many cases are characterized by a superposition of fluvial-channel sediments composed mainly of sandy and gravelly sediments. However, the incised-valley fill formed since the Last Glacial Maximum, the objective of this paper, is relatively complete (Fig. 2). It can be classified into five sedimentary facies that were deposited during the sea-level rise and subsequent stillstand (Figs. 2, 3). In the following text, we will use the newly drilled ZK01 core to describe each facies (Fig. 3).

Facies V (Fluvial Channel Sediments) is bounded by an erosional basal surface and shows a generally upward-fining trend (Figs. 2, 3, 4a). Sediments at the bottom consist mainly of gray or grayish-yellow gravelly sand interbedded by fine sand, silty sand, and gravels (Figs. 3, 4a). The gravels are angular to subangular, with a diameter of 2–50 mm (Fig. 4a), and the sand sediments are primarily composed of coarse (av. 43.4%) and medium (av. 28.8%) sands. The sediments at the top are characterized by an alternation of gray or grayish-yellow silty sand and silty fine sand (Fig. 3). The sediments are well-moderately sorted with a sorting coefficient of 1.14–2.52. Massive,

**Table 1** AMS <sup>14</sup>C ages of organic sediments and shell samples from the newly drilled ZK01 core in the modern Changjiang delta area, China

Lab. code	Depth, m	Materials	Measured <sup>14</sup> C age, yr B.P.	Conventional <sup>14</sup> C age, yr B.P.	Calibrated <sup>14</sup> C age, cal. yr B.P.			
					Age, 1δ	Prob.	Age, 2δ	Prob.
Beta-409604	29.90	Organic sediments	5500 ± 30	5510 ± 30	6300 ± 18	0.95	6310 ± 40 <sup>a</sup>	0.83
Beta-409605	34.60	Shell	3800 ± 30	4200 ± 30	4090 ± 85	1	4100 ± 165	1
Beta-409606	60.00	Organic sediments	11,080 ± 40	11,110 ± 40	13,000 ± 60	1	12,960 ± 120	1
Beta-409607	75.60	Shell	11,790 ± 60	12,170 ± 60	13,470 ± 90	1	13,500 ± 180	1

In this paper, the 2δ calibrated ages are adopted and labeled in Fig. 3

<sup>a</sup> The age is not used because it does not follow the general trend

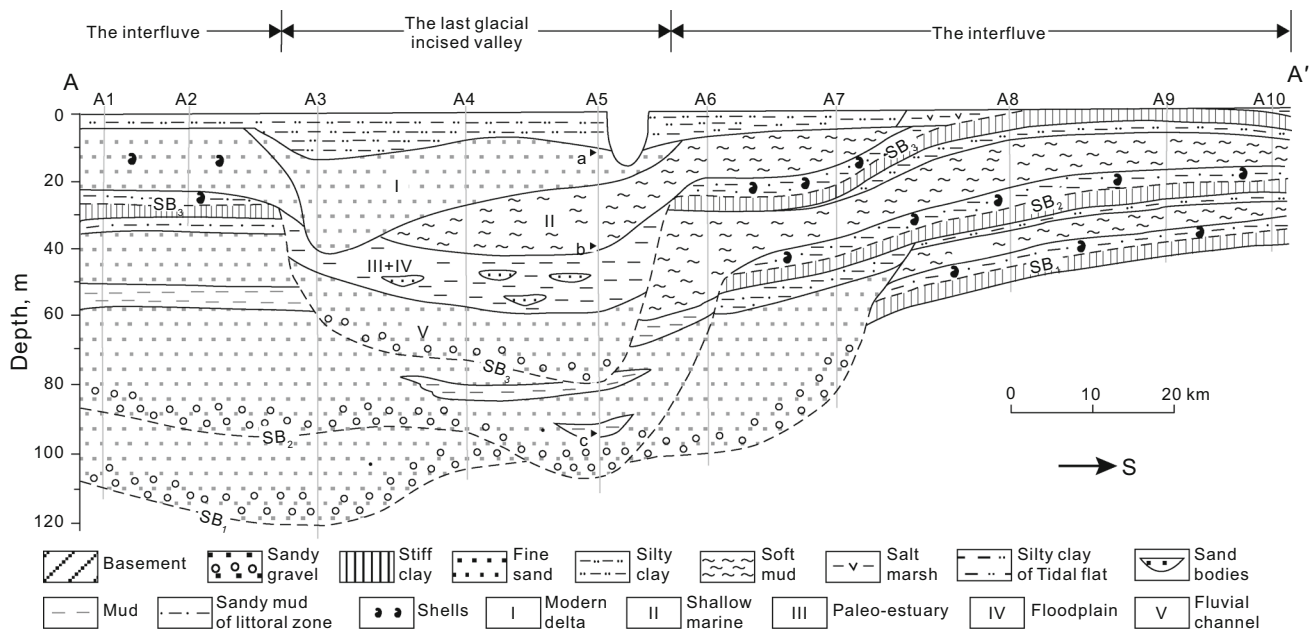


**Fig. 2** Stratigraphic transect (A–A') in the modern Changjiang delta region (modified from Zhang et al. 1998; see Fig. 1a for location). SB: sequence boundary with the subscript indicating the distinct stages for the formation of the Quaternary Changjiang incised valleys.  $^{14}\text{C}$  data were obtained from Li et al. (2002) and calibrated by using

the Calib Rev 7.1 (beta) program (Reimer et al. 2013): a-  $6595 \pm 320$  cal. yr B.P., 11.70 m depth; b-  $12,900 \pm 190$  cal. yr B.P., 38.80 m depth; c-  $39,200 \pm 2200$  cal. yr B.P., 94.50 m depth

graded, and parallel beddings, iron oxide spots, and shells are common, and there is a lack of tide-influenced sedimentary structures. Benthic foraminifera (BF) dominant by *Ammonia beccarii* are identified at the top with nine species and 15 individuals per 50 g (dry weight) sample size. A  $^{14}\text{C}$  date at the burial depth of 75.6 m is  $13,500 \pm 180$  cal. yr B.P. (Fig. 3; Table 1). This facies represents part of the river system and may have been deposited in a channel thalweg to bar environment (cf. Nittrouer et al. 2011; Zhang et al. 2014).

Facies IV (Floodplain Sediments) consists mainly of an alternation of gray mud and grayish-yellow sandy silt, silt, and gravelly sand (Figs. 3 and 4b). The gravels occupying 5%–10% of the coarse sediments have a diameter of 2–5 mm, up to 20 mm. Massive to graded beddings are common in coarse sediments, whereas silty blebs, and massive and lenticular beddings are abundant in mud sediments (Fig. 4b). Only one sample at 68.80 m depth contains some BF with four species and eight individuals per 50 g dry sample size.

Facies III (Paleo-estuary Sediments) is dominated by gray or yellowish-gray mud interbedded by silt and coarse sand with the lamina thickness ranging from 2 mm to 1 m (Fig. 4c). The structureless sand beds are usually typified by an erosional basal surface and present as a fining-upward succession with numerous irregular mud pebbles (Fig. 4d). They are well sorted with a sorting coefficient of 1.52–2.46 and mean grain size of 4.27–6.23  $\Phi$ . Wavy,

horizontal, and massive beddings are common. In addition, a set of tide-influenced sedimentary structures including sand-mud couplet and lenticular bedding are common. Foraminiferal fossils are abundant and mainly composed of BF which consists principally of *Ammonia beccarii* vars., *Florilus decorus*, *Elphidium magellanicum*, *Cribronion vitreum* Wang, and *Elphidium advenum* (Cushman). The number of BF is 14–42 species and 61–10,304 individuals per 50 g dry sample size. A  $^{14}\text{C}$  date of shells at the burial depth of 60.0 m is  $12,960 \pm 120$  cal. yr B.P. (Fig. 3; Table 1). Facies II has been recorded as a macro-tidal system like the Qiantang River estuary with the maximum tidal range located in the Yangzhou area (Li et al. 2006), which is further testified by numerical simulations (Yang and Sun 1988; Uehara et al. 2002).

Facies II (Offshore Shallow Marine Sediments) consists mainly of gray or yellowish-gray soft mud interbedded with gray silt, fine sand, and clayey silt stripes (0.001–0.03 m thick) and blebs (Fig. 4e). Massive, horizontal and lenticular beddings, sand-filled burrows, bioturbation, and seriously broken shells are common (Fig. 4e). Foraminifera are also abundant in this facies and are mainly composed of BF. There are >60 BF species present, including *Ammonia beccarii* vars., *Elphidium magellanicum*, and *Cribronion vitreum* Wang. The number of BF is 27–44 species and 139–5888 individuals, respectively, based on 50 g (dry weight) sample size. The foraminiferal fossils in Facies II resemble the living groups

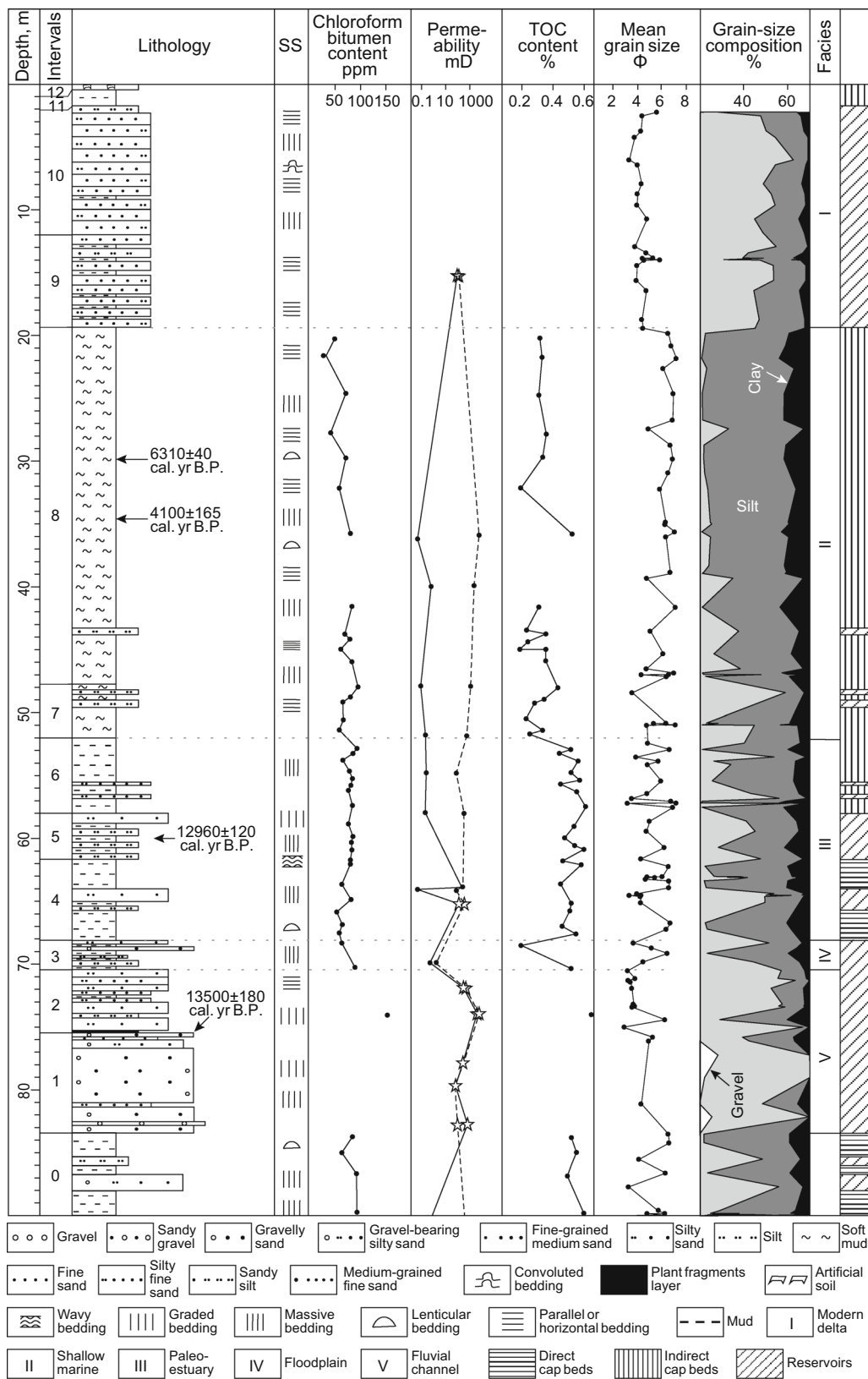


**Fig. 3** Columnar section of core ZK01 in the modern Changjiang delta area (see Fig. 1 for location). *Black circles* indicate the depths at which various features were observed, and *light stars* show the

sediment samples of reservoirs. In the column of permeability, the *dashed line* indicates horizontal permeability, while the *solid line* indicates vertical permeability. SS: sedimentary structure

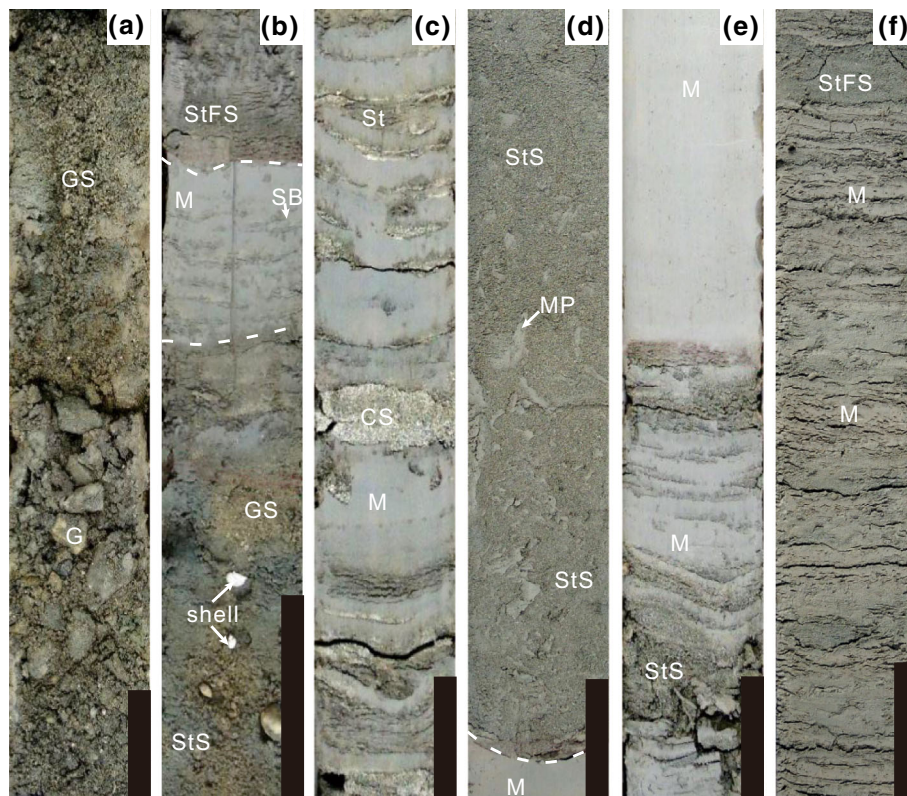


**Fig. 4** Photographs of typical sedimentary characteristics in the ZK01 core. *Black scale bar = 10 cm.* **a** Facies V, 82.30–82.80 m depth: grayish-yellow gravelly sand (GS) with graded bedding. **b** Facies IV, 68.45–68.80 m depth: alternation of gray mud (M) and grayish-yellow silty fine sand (StFS), silty sand (StS), and gravelly sand with the lithological unconformity surface indicated by a white dotted line. Lenticular bedding and silty blebs (SB) are common in the mud sediments, while graded and massive bedding and shells are present in the sand sediments. **c** Facies III, 66.35–66.70 m depth: gray

mud interbedded by thin silt (St) and coarse sand (CS) layers. **d** Facies III, 58.40–58.85 m depth: gray silty sand with an erosional basal surface (white dashed line) and numerous irregular mud pebbles (MP), present as a fining-upward succession. **e** Facies II, 57.30–57.80 m depth: alternation of gray mud and silty sand at the bottom and then massive gray soft mud at the top. **f** Facies I, 17.30–17.80 m depth: alternation of gray silty fine sand and mud. G: gravel

in the offshore shallow water areas (<20–55 m) of the East China Sea, South Yellow Sea, Changjiang delta, and Bohai Bay (Wang et al. 1981; Li and Wang 1998; Zhuang et al. 2002; Li et al. 2002; Li et al. 2010b).

Facies I (Modern Delta Sediments) shows an upward-coarsening sequence. The sediments at the bottom are characterized by an alternation of silty fine sand and mud (Figs. 3, 4f). The sand beds (0.3–7 cm thick) consist mainly of fine sand (52%–67%) and silt (29%–42%) with a mean grain size of 3.8–4.5  $\Phi$  and are well sorted with a sorting coefficient <2, while the mud sediments (0.1–3 cm thick) dominated by silt and clay. The sediments at the top consist predominantly of gray sand interbedded by gray or brown mud stripes (0.5–3 cm thick) or muddy gravels (Fig. 3). The sand sediments are mainly composed of fine sand (50.3%–75.8%) and silt (13.6%–37.7%), with a mean grain size of 3.3–4.4  $\Phi$  and sorting coefficient of 1.3–2.2. Parallel, massive, and convolute beddings, as well as seriously broken shells, are common (Fig. 3).

Foraminiferal fossils dominated by BF (>58 species; >42,688 in a 50-g dry sample) are also abundant in this facies. Most BF individuals are juveniles with small and/or seriously abraded shells. The BF assemblage of this facies, including *Ammonia beccarii* vars., *Elphidium naraensis*, *Florilus decorus*, *Protelphidium tuberculatum* (d'Orbigny), and *Elphidium magellanicum*, is similar to that of the modern Changjiang delta (cf. Li and Wang 1998).

## 5 Characteristics of shallow biogenic-gas reservoirs

### 5.1 Biogenic origin of shallow gas

Table 2 presents the chemical and isotopic compositions of the shallow gas in the study area. Results show that most of the gas samples are dominated by CH<sub>4</sub> (generally >95%), with minor N<sub>2</sub> (0.75%–9.07%) and CO<sub>2</sub> (0.98%–3.23%).

The gas sample from CPT-1 (see Fig. 1b for location) is special in consisting mainly of N<sub>2</sub> (64.0%) and CH<sub>4</sub> (23.5%). The carbon isotope values of CH<sub>4</sub> and CO<sub>2</sub> are −75.8 to −67.7‰ and −34.5 to −6.6‰, respectively, and the hydrogen isotope values of CH<sub>4</sub> are −215 to −185‰. These results indicate a biogenic origin for the shallow gas (cf. Whiticar et al. 1986; Whiticar 1999; Humez et al. 2016; Tao et al. 2016; Sun et al. 2016). The nitrogen-rich biogenic gas may be derived from the degradation of nitrogen-rich organic matter, indicating that the organic matter of the source sediments in the study area is heterogeneous (cf. Wang 1982). In addition, all the gases plot within “Bacterial Carbonate Reduction” zone in Fig. 5, indicating that the methanogenesis is predominant from carbon dioxide reduction (cf. Whiticar et al. 1986).

### 5.2 Gas-source sediments

There are three potential kinds of gas-source sediments in this area, including the gray and light-brown mud of Facies IV, gray and yellowish-gray mud of Facies III, gray and yellowish-gray soft mud of Facies II (Figs. 2, 3). Mud beds of Facies I can be excluded because they are thin (<0.5 m) and close to the surface (Figs. 2, 3).

Systematic analysis of core ZK01 indicates that TOC content increases with depth, and the argillic sediments of Facies III and IV have higher TOC contents than those of Facies II (Fig. 3). The TOC contents of Facies III and IV exceed the lower limits for both terrestrial (0.18%, Zhou et al. 1994) and marine gas sources (0.5%; Rice and Claypool 1981), whereas those of Facies II are below the lower limit for potential marine gas sources (Table 3). The chloroform bitumen content of source sediments shows a similar variation trend among distinct sedimentary facies (Fig. 3; Table 3).

Pyrolysis results show that the Tmax values are generally <435 °C, the gas generation potential index ranges from 0.09 to 0.19 mg/g sediment, and the hydrogen index

values vary from 15.97 to 42.48 mg/g TOC (Table 4), implying that the organic materials are substantial at the immature stage and the biogas is now still being formed at a massive generation stage (cf. Lin et al. 2004; Zhang et al. 2013). H/C and O/C ratios of kerogen vary in a range of 0.89–1.25 and 0.27–0.38, respectively, and plot in the type III kerogen area (gas prone; cf. Peters et al. 1986; Fig. 6), which are supported by the correlation of Tmax and HI indexes.

In summary, the argillic sediments of Facies III and IV are more likely to act as effective gas-source sediments (cf. Zhang and Chen 1983; Lu and Hai 1991; Wu et al. 2014). However, the TOC contents and chloroform bitumen values for the argillic sediments in the study area are significantly lower than those from the nearby Qiantang River

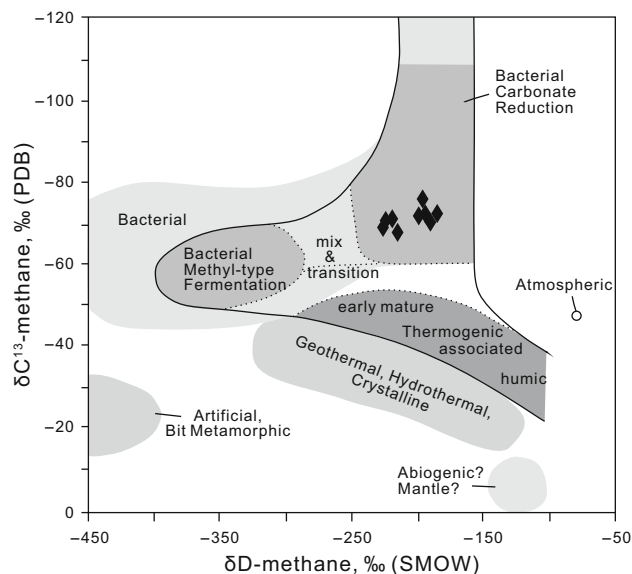


**Fig. 5** Cross plot of δ<sup>13</sup>C and δD of the methane for the shallow gas in the modern Changjiang delta area, eastern China, implying gases generated through the pathway of H<sub>2</sub> reduction of CO<sub>2</sub> (base diagram is from Whiticar 1999)

**Table 2** Geochemical characteristics of the shallow gas in the Qidong area of the modern Changjiang delta region, China

CPT	Depth, m	Chemical composition, %					δ <sup>13</sup> C <sub>CH4</sub> PDB, ‰	δ <sup>13</sup> C <sub>CO2</sub> PDB, ‰	δD <sub>CH4</sub> SMOW, ‰
		CH <sub>4</sub>	C <sub>2</sub> H <sub>6</sub>	CO <sub>2</sub>	CO	N <sub>2</sub>			
1	70	23.6	u.d.	1.5	10.9	64.0	−67.7	−19.3	−215
3	20	87.7	u.d.	3.2	u.d.	9.1	−71.7	−34.5	−199
	70	96.2	u.d.	1.8	u.d.	2.0	−72.2	−20.4	−194
4	62	98.1	u.d.	1.2	u.d.	0.8	−70.2	−6.6	−190
13	40	97.7	u.d.	1.3	u.d.	1.0	−72.3	−21.4	−185
	70	95.1	u.d.	1.1	u.d.	3.7	−75.8	−21.4	−196

Note: *u.d.* under detection limit

**Table 3** Organic matter abundance of the mud sediments from the different sedimentary facies of cores ZK01 and ZK02 in the modern Changjiang delta area, China

Facies	Depth, m	Lithology	TOC content, wt. %			Chloroform bitumen content, ppm		
			Min.	Max.	Av.	Min.	Max.	Av.
II	20.30–51.40	Gray soft mud	0.19	0.52	0.32 (17)	32	95	67 (17)
III	52.90–67.60	Gray or yellowish-gray mud	0.44	0.61	0.52 (21)	53	93	76 (21)
IV + V	68.40–74.10	Light-brown or gray mud	0.20	0.65	0.46 (3)	63	153	102 (3)

Numbers in parentheses = sample number of analyses

Note: *Min.* minimum, *Max.* maximum, *Av.* average

**Table 4** Pyrolysis results of the gas-source sediments from different sedimentary facies of cores ZK01 and ZK02 in the modern Changjiang delta area, China

Facies	Lithology	Depth, m	$S_1$ , mg/g	$S_2$ , mg/g	Gas generation potential ( $S_1 + S_2$ ), mg/g	Hydrogen index, mg/g	$T_{max}$ , °C
II	Gray soft mud	24.7	0.02	0.07	0.09	22.74	463
		29.2	0.01	0.07	0.08	15.97	429
		48.0	0.03	0.13	0.16	30.15	394
III	Gray mud	63.7	0.05	0.14	0.19	31.25	424
		40.9	0.03	0.15	0.18	35.30	387
		45.1	0.03	0.15	0.18	42.48	439

Note:  $S_1$  the amount of free hydrocarbons volatilized from the sediment sample,  $S_2$  the hydrocarbons produced by cracking of organic matter in the sediment sample, *Hydrogen index* ( $S_2/TOC$ )  $\times$  100,  $T_{max}$  = the temperature of the maximum  $S_2$  yield

incised-valley fill (cf. Lin et al. 2004; Zhang et al. 2013), which may be caused by the remarkably different amount of terrigenous sediment inputs. The mean annual suspended sediment load is  $\sim 4.8 \times 10^8$  t/yr for the Changjiang, generally two orders of magnitude higher than that of the Qiantang River ( $\sim 0.09 \times 10^8$  t/yr). This huge terrigenous sediment input dilutes the organic matter abundance, as a result implying that the mud sediments in the postglacial Changjiang incised-valley fill have a relatively lower biogas generation potential than those in the Qiantang River incised-valley fill.

### 5.3 Reservoirs

The potential shallow biogenic-gas reservoirs in the study area can be classified into five types (Figs. 3, 7): (a) beds of sandy gravel, gravelly sand, medium-grained fine sand, and silty sand of Facies V; (b) sand bodies of Facies IV composed mainly of silty sand, sandy silt, and silt; (c) sand bodies of Facies III characterized by silty sand and sandy silt; (d) lenses of sand (silty fine sand, sandy silt, silt, and clayey silt) intercalated in the soft mud of Facies II; and (e) silty fine sand and sandy silt in Facies I. Based on the available exploration data, commercial gas was

encountered mainly in the sand bodies of Facies III and IV and secondarily in the top parts of the sand beds of Facies V (Figs. 3, 7). The sand bodies of Facies II are thin with a thickness of 0.005–0.95 m (generally  $<0.5$  m; Figs. 3, 4e, 7). Although the sand sediments of Facies I are thick and composed mainly of coarse grains, the attributes including being close to the surface and lack of effective cap beds (0.1–3 m thick) make them unsuitable to be effective reservoirs in the study area (Fig. 3).

Therefore, determining the size, shape, and permeability of the sand bodies in Facies III, IV, and V is essential for exploration prediction and exploitation of shallow biogenic gas in the study area. The sand bodies in Facies III and IV vary significantly in thickness (0.5–4.0 m) and burial depth (50–70 m). Even in neighboring boreholes, the depth difference may be over 3–4 m (Fig. 7). In some cases, a borehole can go through up to  $>10$  layers of sand with a total thickness of  $\sim 20$  m (Fig. 7), but no sand layers are penetrated by the neighboring borehole. All the sand bodies are encased entirely by mud and vary in size (Fig. 7). Small bodies are distributed locally, but large ones can extend up to several hundreds of meters. The vertical permeabilities of the sand bodies in Facies III are of 122.9–211.5 mD, generally lower than the horizontal permeabilities

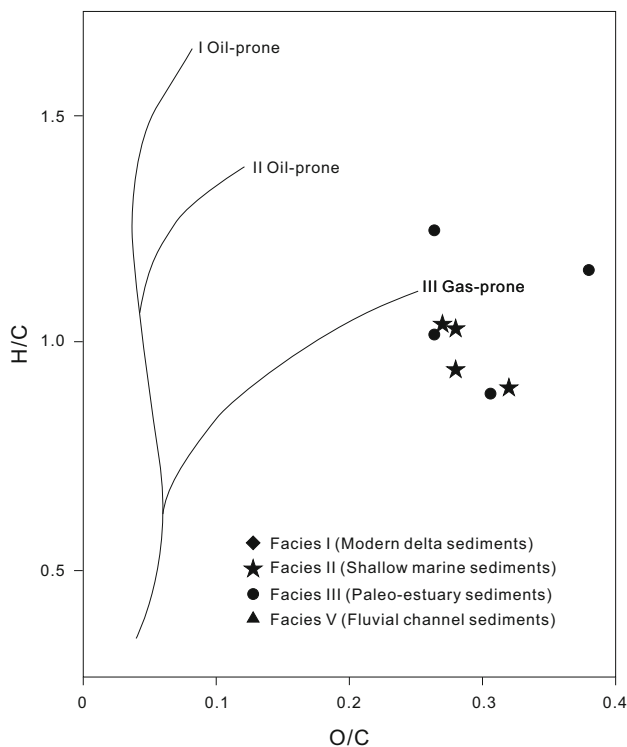


**Fig. 6** Plot of H/C vs. O/C ratios (according to Peters et al. 1986) implying the kerogen character for the mud sediments in the late Quaternary Changjiang incised valley

(273.3–352.5 mD, Table 5), which may be influenced by the heterogeneity of sand bodies, for instance, the presence of parallel bedding and mud clasts (Figs. 4d, 8a). Generally speaking, the size, thickness, and permeability of the sand bodies in the study area are considerably lower than those of the sand bodies from the same facies in the late Quaternary Qiantang River incised-valley fill (Zhang et al. 2013, 2014). The sand bodies in Facies III of the Qiantang River incised-valley fill are characterized by a thickness of 3–20 m, burial depth of 28–78 m, width of 0.4–2 km, and permeability of 577–4,590 mD (Zhang et al. 2013, 2014).

The potential shallow biogenic-gas reservoirs in Facies V occur in the local highs, which are capped directly by the mud of Facies IV, and have a burial depth of 58–70 m (Fig. 7). The local highs, which are surrounded by fluvial-channel sand sediments formed in the previous incised-valley period however, cannot become effective gas reservoirs (Fig. 9). Permeabilities of these sand reservoirs (66.99–15,037.03 mD) are generally higher than those of sand bodies in Facies III and IV, which may be caused by the coarser grain size and lower contents of mud (Fig. 8b); nevertheless, they are characterized by a complex difference between the vertical and horizontal permeabilities, i.e., sometimes vertical permeability is higher than the horizontal, and *vice versa* (Table 5).

## 5.4 Cap beds

In the study area, commercial gas-bearing pools mainly occur as sand bodies capped directly by the mud beds of Facies III and IV, which are restricted within the incised valley (burial depth of 30–90 and thickness of 10–18 m) and are called direct or local cap beds (Figs. 2, 3, 9). By contrast, the soft mud covering the whole incised valley and deposited in an offshore shallow marine environment is called regional or indirect cap beds with a burial depth of 10–60 m and thickness of 5–20 m (Figs. 2, 3, 9). This is similar to that of the Qiantang River incised valley. Zhang et al. (2013) proposed that capillary sealing, pore-water pressure sealing, and hydrocarbon concentration sealing are considered as the main mechanisms for the conservation of the shallow biogenic gas in the Qiantang River incised-valley area. In this paper, we use vertical permeability, which has a negative relationship with the capillary sealing capacity of cap beds, to indirectly illustrate the sealing mechanism of cap beds. The vertical permeabilities of cap beds (0.05–0.52 mD) are significantly lower than those of sand reservoirs (66.99–15037 mD) with a difference of 4–6 orders of magnitude, which makes cap beds effective in preventing gas escaping from reservoirs (Table 5).

The vertical permeabilities have a similar variation trend with the contents of sand and silt, but an inverse correlation with the mud content (Fig. 3). The cap beds composed mainly of mud have the lowest permeability, and the vertical permeability is generally equal to the horizontal one, whereas those with sand bands or inclusions are marked by higher permeabilities, and the horizontal permeabilities are significantly higher than the vertical ones, by about 3–4 orders of magnitude (Figs. 3, 8c, d, e, f; Table 5). This result indicates that mud content plays a significant role in the capillary sealing ability of cap beds, namely the massive mud has much stronger sealing ability.

## 5.5 Gas migration and accumulation model

Methane is predominantly dissolved in the water within gas-source beds, with less being absorbed by clay minerals, and free gas is present only when saturation is attained with increasing depth of burial (cf. Lin et al. 2004; Gao et al. 2010, 2012). As a result, most gas in the study area is regarded as being transported from gas-source beds to sand beds by formation water with the differential compaction between sand and mud beds. Also, the capillary pressure difference between gas-source beds and sand reservoirs indicated by the huge difference in vertical permeability (Table 5) also drives gas migrating from mud beds to sandy reservoirs (cf. Magara 1987). After gas is released from mud sediments, it can migrate toward the overlying,

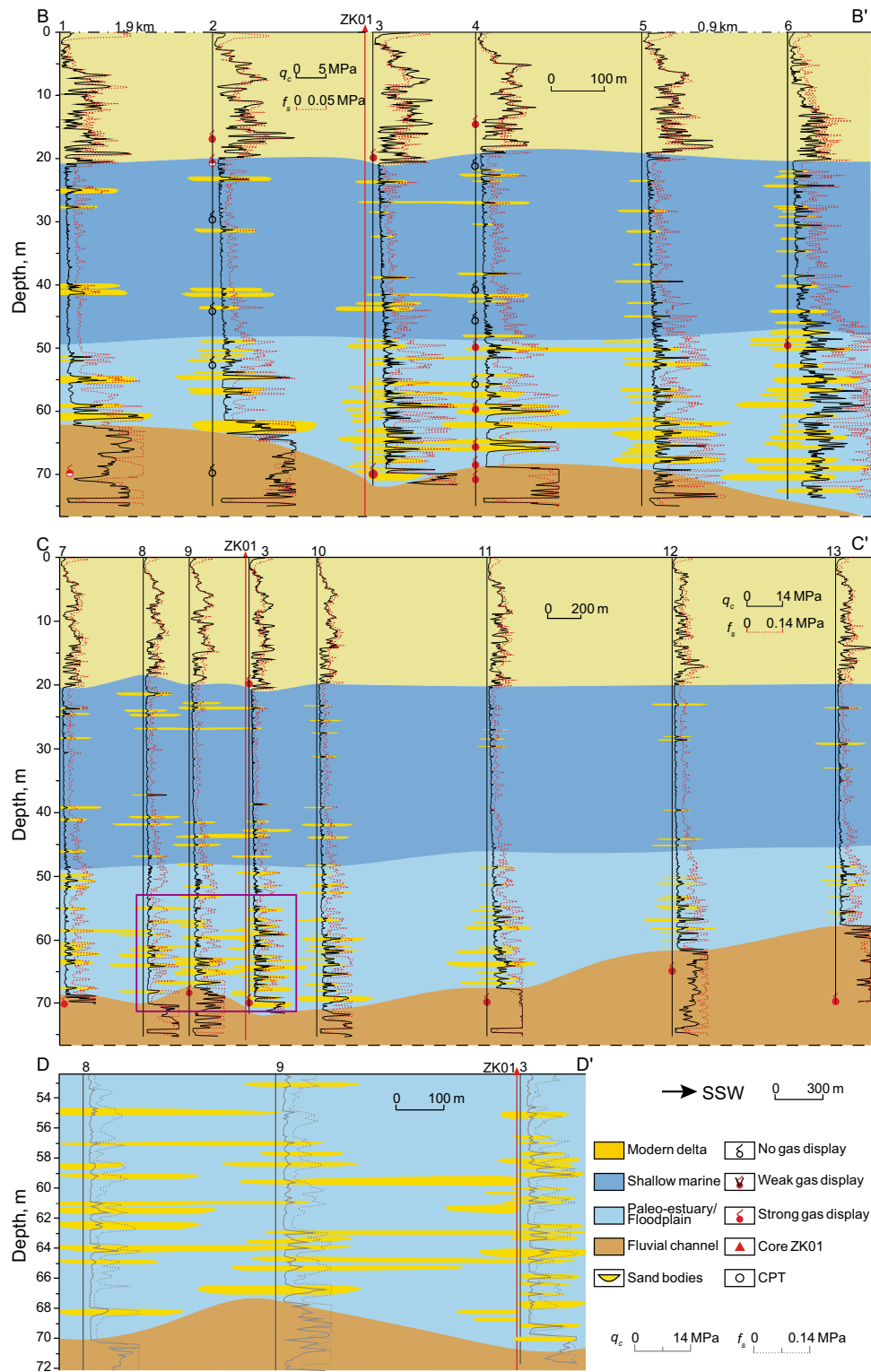


**Fig. 7** Contrast of different CPTs in the Qidong area from the modern Changjiang delta region showing the distribution pattern of the sand beds in different facies. See Fig. 1 for locations. Profile **D–D'** is a close-up view of the purple box area in the profile **C–C'**

underlying, or lateral sand bodies (Fig. 9). Within sand reservoirs, the methane-filled space is initially restricted to the top, but it expands downward when methane is

abundant, and the formation water is expelled along the gas–water interface. In addition, gas migrates more frequently and easily along the bedding surface than in the

**Table 5** Permeabilities of the cap beds and reservoirs of core ZK01 in the modern Changjiang delta area, China

Facies	Depth, m	Lithology	Vertical permeability, mD	Horizontal permeability, mD	Reservoirs
I	13.80–14.00	Alternation of silty fine sand and sandy silt	82.14–101.80/89.78(6 <sup>a</sup> )	115.37–136.25/124.46(6)	Reservoirs
II	34.80–35.00	Soft mud	0.04–0.05/0.05(3)		Indirect cap beds
	38.80–39.00	Soft mud with thin-bedded silt and silt blocks	0.43–0.80/0.59(3)	2,245.92–2,365.12/2,312.70(6)	
III	46.80–47.00	Alternation of silty fine sand and soft mud	0.08–0.09/0.08(3)	1,059.74–1,294.41/1,171.16(6)	
	50.80–51.00	Soft mud with thin-bedded sandy silt	0.20–0.21/0.20(3)	456.23–640.49/552.44(6)	
	53.80–54.00	Mud with horizontal bedding	0.22–0.24/0.23(3)	58.34–113.20/75.88(6)	Direct cap beds
	57.00–57.20	Mud with sandy and silty blocks	0.19–0.21/0.20(3)	236.73–409.30/333.07(7)	
	63.00–63.20	Sandy silt with parallel bedding	169.08–234.65/211.54(6)	256.43–302.87/273.32(6)	Reservoirs
IV	63.20–63.40	Mud with horizontal bedding	0.05–0.05/0.05(3)	8.82–207.28/70.17(6)	Direct cap beds
	64.35–64.55	Massive silty fine sand with mud blocks	99.87–170.37/122.88(7)	224.15–538.04/352.49(6)	Reservoirs
V	69.05–69.25	Mud	0.45–0.53/0.48(3)	1.43–1.62/1.49(3)	Direct cap beds
	71.10–71.30	Massive silty sand	237.19–425.86/279.66(7)	232.86–874.42/463.67(6)	Reservoirs
	73.15–73.35	Massive silty sand	3933.75–4235.73/4039.75(6)	5,723.47–6,287.39/6,019.80(6)	
	77.20–77.40	Gravelly sand	253.29–272.28/263.40(6)	272.28–316.94/304.09(6)	
	79.00–79.20	Slightly gravelly sand	62.91–75.38/66.99(6)	54.78–67.03/60.18(6)	
	82.10–82.30	Gravelly sand	548.25–798.87/652.45(6)	86.07–109.68/94.18(6)	

Note: 82.14–101.80/89.78 shows the minimum–maximum/average values

<sup>a</sup> Numbers in parentheses = number of analyses for one sample

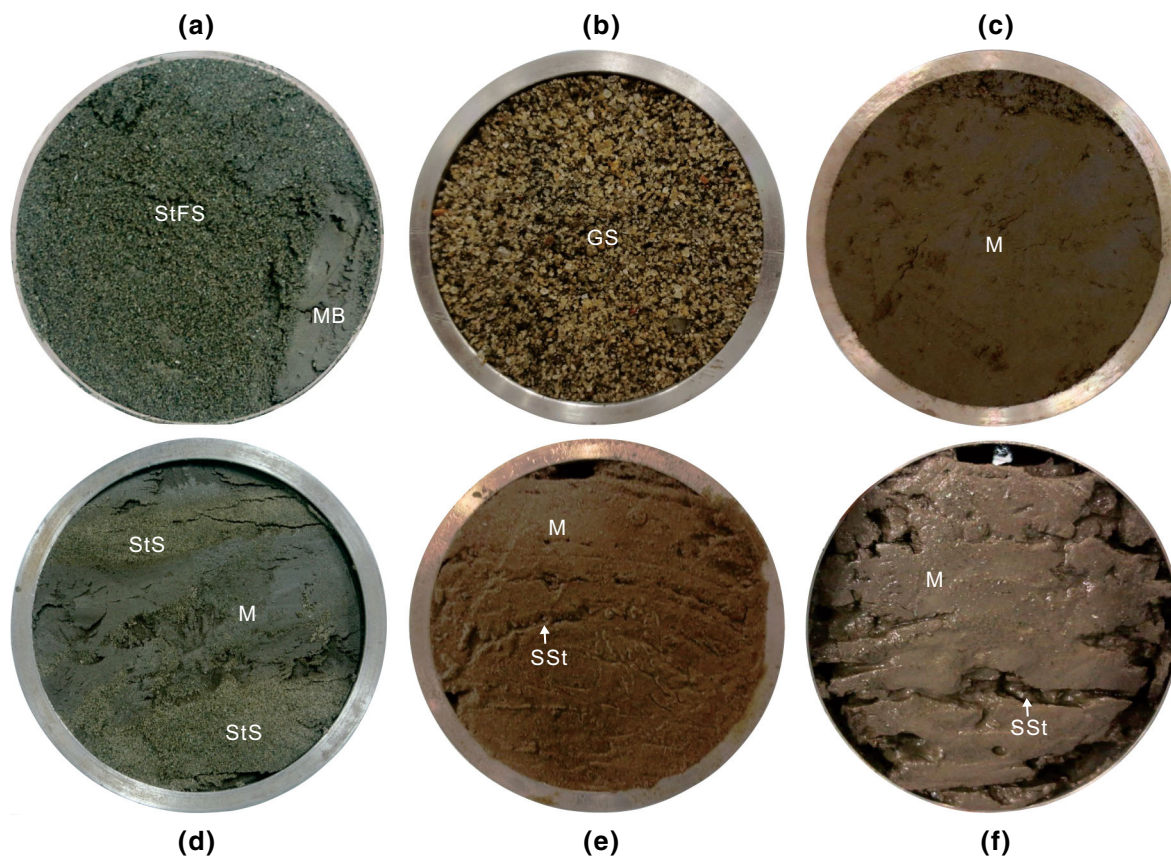


**Fig. 8** Photographs showing the typical sedimentary characteristics of permeability samples. **a** 64.35–64.55 m depth: massive silty fine sand (StFS) with mud blocks (MB), *vertical* permeability of 123 mD, and *horizontal* permeability of 352 mD. **b** 77.20–77.40 m depth: structureless gravelly sand (GS) with *vertical* and *horizontal* permeabilities of 263 and 304 mD, respectively. **c** 69.05–69.25 m depth: massive mud (M) with *vertical* permeability of 0.48 mD and

*horizontal* permeability of 1.49 mD. **d** 89.80–90.00 m depth: alternation of mud and silty sand (StS) with *vertical* and *horizontal* permeabilities of 0.52 and 395.6 mD, respectively. **f** and **e** 50.80–51.00 m depth: mud with thin-bedded sandy silt (SSt), *vertical* permeability of 0.20 mD, and *horizontal* permeability of 552 mD; the sand beds have been washed away after experiment

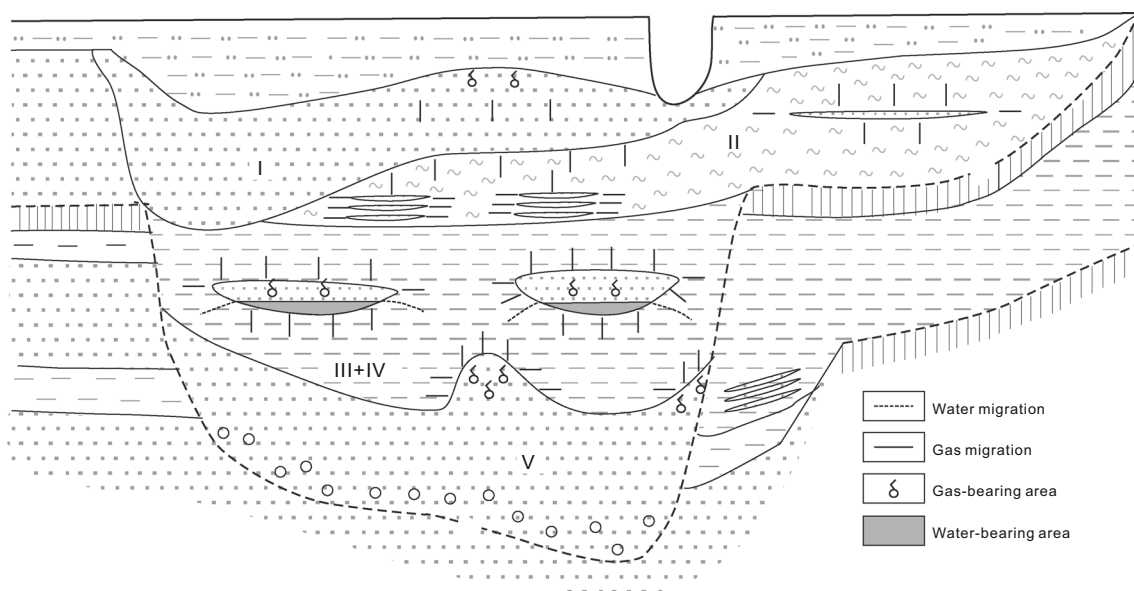


**Fig. 9** Accumulation model of the shallow biogenic gas in the postglacial Changjiang incised-valley fill. See legends in Fig. 2

direction perpendicular to it within gas-source layers indicated by the difference between vertical and horizontal permeabilities (Table 5; Fig. 3).

As neotectonism in the study area is only characterized by uplift of the hilly lands and subsidence (1–3 mm/yr) in the coastal plain area (Chen and Stanley 1993), gas-bearing strata in the Changjiang delta area remain horizontal; therefore, gas migration and accumulation are mainly controlled by the lithology of gas-source layers and reservoirs, and there are no significant structural traps. As a consequence, sand bodies of Facies III and IV provide optimum conditions for in situ stratigraphic entrapment of biogenic gas and secondly in local highs of Facies V.

## 6 Conclusions

The natural gas in the modern Changjiang delta area consists primarily of CH<sub>4</sub> (generally >95%) and has a biogenic origin with carbon isotope ratios of CH<sub>4</sub> and CO<sub>2</sub> of −75.8 to −67.7‰ and −34.5 to −6.6‰, respectively, and hydrogen isotope ratios of CH<sub>4</sub> of −215 to −185‰. It is mainly distributed in the postglacial Changjiang incised-valley fill, which consists principally of five sedimentary facies in ascending order, i.e., fluvial channel (Facies V), floodplain (Facies IV), paleo-estuary (Facies III), offshore shallow marine (Facies II), and modern delta (Facies I). The sand bodies of Facies III and IV and local highs of Facies V are primary potential gas reservoirs. The former vary significantly in thickness (0.5–4.0 m) and burial depth (50–70 m), and the latter with a thickness larger than 10 m and burial depth of 58–70 m (Fig. 7). The main gas sources are gray or yellowish-gray mud of Facies III and IV, and the organic matter is dominated by type III kerogen (gas prone) at an immature stage. Meanwhile, the gas sources occur as cap beds, and the mud sediments of Facies III and IV that encase sand reservoirs directly are referred as direct cap beds, while the soft mud of Facies II called indirect ones. The huge difference in vertical permeability, about 4–6 orders of magnitude, between cap beds and reservoirs allows cap beds to effectively reduce the upward escape of gas in reservoirs. Therefore, it is notable that the shallow biogenic-gas reservoirs in the study area are of classic “self-generated and self-reserved” lithological entrapment type, and the sand bodies of Facies III, IV, and V should be considered as promising targets for exploration.

**Acknowledgements** This work was supported by the National Natural Science Foundation of China under Grant Numbers 41402092 and 41572112, the Natural Science Foundation (Youth Science Fund Project) of Jiangsu Province (BK20140604), and the Scholarship under State Scholarship Fund sponsored by the China Scholarship Council (File No. 201506195035). We thank C. Liu, Y.M., Jiang, H. Wang, J. Yu, C.W. Deng, Q.C. Yin, C. Lu, and Q. Wang for their

helpful discussions, and assistance in field and core observations, and sample analyses. Special thanks should be extended to Dr. X.W. Sun of Sun Petroleum Geoservices, Australia, and Dr. J. Cao of Nanjing University for checking the English presentation. We also thank Dr. Y.H. Shuai of the PetroChina Research Institute of Petroleum Exploration and Development, China, anonymous reviewers and Petroleum Science editors for their constructive suggestions and comments.

**Open Access** This article is distributed under the terms of the Creative Commons Attribution 4.0 International License (<http://creativecommons.org/licenses/by/4.0/>), which permits unrestricted use, distribution, and reproduction in any medium, provided you give appropriate credit to the original author(s) and the source, provide a link to the Creative Commons license, and indicate if changes were made.

## References

- Blott SJ, Pye K. Gradistat: a grain size distribution and statistics package for the analysis of unconsolidated sediments. *Earth Surf Proc Land*. 2001;26(11):1237–48.
- Chen ZY, Stanley DJ. Yangtze delta, eastern China: 2. Late Quaternary subsidence and deformation. *Mar Geol*. 1993;112:13–21.
- Dalrymple RW, Boyd R, Zaitlin BA. History of research, types and internal organization of incised-valley systems: introduction to the volume. In: Dalrymple RW, Boyd R, Zaitlin BA, editors. *Incised-valley systems: origin and sedimentary sequences*. SEPM Spec. Publ.; 1994; 51:3–10.
- Gao G, Huang ZL, Huang BJ, et al. The solution and exsolution characteristics of natural gas components in water at high temperature and pressure and their geological meaning. *Pet Sci*. 2012;9(1):25–30.
- Gao Y, Jin Q, Zhu GY. Genetic types and distribution of shallow-buried natural gases. *Pet Sci*. 2010;7(3):347–54.
- García-García A, Orange DL, Miserocchi S, et al. What controls the distribution of shallow gas in the Western Adriatic Sea? *Cont Shelf Res*. 2007;27(3–4):359–74.
- García-Gil S, Vilas F, García-García A. Shallow gas features in incised-valley fills (Ría de Vigo, NW Spain): a case study. *Cont Shelf Res*. 2002;22(16):2303–15.
- Heggland R. Detection of gas migration from a deep source by the use of exploration 3D seismic data. *Mar Geol*. 1997;137(1–2):41–7.
- Hori K, Saito Y, Zhao QH, et al. Architecture and evolution of the tide-dominated Changjiang (Yangtze) River delta, China. *Sedim Geol*. 2002;146(3–4):249–64.
- Hori K, Saito Y, Zhao QH, et al. Sedimentary facies and Holocene progradation rates of the Changjiang (Yangtze) delta, China. *Geomorphology*. 2001;41(2–3):233–48.
- Humez P, Mayer B, Ing J, et al. Occurrence and origin of methane in groundwater in Alberta (Canada): gas geochemical and isotopic approaches. *Sci Total Environ*. 2016;541:1253–68.
- Jones KL, Lindsay MJB, Kipfer R, et al. Atmospheric noble gases as tracers of biogenic gas dynamics in a shallow unconfined aquifer. *Geochim Cosmochim Acta*. 2014;128:144–57.
- Li CX, Chen QQ, Zhang JQ, et al. Stratigraphy and paleoenvironmental changes in the Yangtze Delta during the Late Quaternary. *J Asian Earth Sci*. 2000;18(4):453–69.
- Li CX, Wang PX. *Researches on Stratigraphy of the Late Quaternary Period in Yangtze River Mouth*. Beijing: Science Press; 1998 (**in Chinese**).
- Li CX, Wang P, Fan DD, et al. Characteristics and formation of late Quaternary incised-valley-fill sequences in sediment-rich deltas

- and estuaries: case studies from China. In: Dalrymple RW, Leckie DA, Tillman RW, editors. *Incised valleys in time and space*, vol. 85. SEPM Spec. Publ; 2006. p. 141–60.
- Li CX, Wang P, Sun HP, et al. Late Quaternary incised-valley fill of the Yangtze delta (China): its stratigraphic framework and evolution. *Sedim Geol.* 2002;152(1–2):133–58.
- Li P, Du J, Liu LJ, et al. Distribution characteristics of the shallow gas in Chinese offshore seabed. *Chin J Geol Hazard Control.* 2010a;21(1):69–74 (in Chinese).
- Li XY, Shi XF, Cheng ZB, et al. Distribution of benthic foraminifera in surface sediments of the Laizhou Bay, Bohai Sea and its environmental significance. *Acta Micropalaeontol Sin.* 2010b;27:38–44 (in Chinese).
- Li YL, Lin CM. Exploration methods for late Quaternary shallow biogenic gas reservoirs in the Hangzhou Bay area, eastern China. *AAPG Bull.* 2010;94:1741–59.
- Lin CM, Gu LX, Li GY, et al. Geology and formation mechanism of late Quaternary shallow biogenic gas reservoirs in the Hangzhou Bay area, eastern China. *AAPG Bull.* 2004;88(5):613–25.
- Lin CM, Li YL, Zhuo HC, et al. Features and sealing mechanism of shallow biogenic gas in incised valley fills (the Qiantang River, eastern China): a case study. *Mar Pet Geol.* 2010;27(4):909–22.
- Lin CM, Zhang X, Xu ZY, et al. Sedimentary characteristics and accumulation conditions of shallow-biogenic gas for the Late Quaternary sediments in the Changjiang River delta area. *Adv Earth Sci.* 2015;30(5):589–601 (in Chinese).
- Liu CL, Zhu J, Che CB, et al. Potential recoverable natural gas resources in China. *Pet Sci.* 2008;5(1):83–6.
- Lu WW, Hai XZ. Simulation experiments on biogenic gas generation and estimation of generation amount of biogenic gas in strata. *Exp Pet Geol.* 1991;13:65–75 (in Chinese).
- Magara K. *Compaction and fluid migration*. Amsterdam-Oxford, New York: Elsevier Scientific Publishing Company; 1987. p. 319.
- Milliman JD, Syvitski JPM. Geomorphic/tectonic control of sediment discharge to the ocean: the importance of small mountainous rivers. *J Geol.* 1992;100(5):525–44.
- Moran K, Hill PR, Blasco SM. Interpretation of piezocone penetrometer profiles in sediment from the Mackenzie Trough, Canadian Beaufort Sea. *J Sedim Res.* 1989;59:88–97.
- Ni YY, Dai JX, Zou CN, et al. Geochemical characteristics of biogenic gases in China. *Int J Coal Geol.* 2013;113:76–87.
- Nittroer JA, Mohrig D, Allison MA, et al. The lowermost Mississippi River: a mixed bedrock-alluvial channel. *Sediment.* 2011;58(7):1914–34.
- Okay S, Aydemir S. Control of active faults and sea level changes on the distribution of shallow gas accumulations and gas-related seismic structures along the central branch of the North Anatolian Fault, Southern Marmara shelf, Turkey. *Geodinamica Acta.* 2016;28:328–46.
- Peters KE, Moldowan JM, Schoell M, et al. Petroleum isotopic and biomarker composition related to source rock organic matter and depositional environment. *Org Geochem.* 1986;10(1–3):17–27.
- Pinet N, Duchesne M, Lavoie D, et al. Surface and subsurface signatures of gas seepage in the St. Lawrence Estuary (Canada): significance to hydrocarbon exploration. *Mar Pet Geol.* 2008;25(3):271–88.
- Reimer PJ, Bard E, Bayliss A, et al. IntCal13 and Marine-13 radiocarbon age calibration curves 0–50,000 years cal BP. *Radiocarbon.* 2013;55(4):1869–87.
- Rice DD, Claypool GE. Generation, accumulation, and resource potential of biogenic gas. *AAPG Bull.* 1981;65(1):5–25.
- Rogers JN, Kelley JT, Belknap DF, et al. Shallow-water pockmark formation in temperate estuaries: a consideration of origins in the western gulf of Maine with special focus on Belfast Bay. *Mar Geol.* 2006;225(1–4):45–62.
- Stanley DJ, Chen ZY. Neolithic settlement distributions as a function of sea level-controlled topography in the Yangtze delta, China. *Geology.* 1996;24(12):1083–6.
- Stax R, Stein R. Long-term changes in accumulation of organic carbon in Neogene sediments of ODP-Leg 130 (Ontong Java Plateau). *Proc ODP Sci Results.* 1993;130:573–84.
- Sun PA, Wang Y, Leng K, et al. Geochemistry and origin of natural gas in the eastern Junggar Basin, NW China. *Mar Pet Geol.* 2016;75:240–51.
- Tao KY, Cao J, Wang Y, et al. Geochemistry and origin of natural gas in the petroliferous Mahu sag, northwestern Junggar Basin, NW China: carboniferous marine and Permian lacustrine gas systems. *Org Geochem.* 2016;100:62–79.
- Uehara K, Saito Y, Hori K. Paleotidal regime in the Changjiang (Yangtze) estuary, the East China Sea, and the Yellow Sea at 6 ka and 10 ka estimated from a numerical model. *Mar Geol.* 2002;183(1–4):179–92.
- Vielstädte L, Karstens J, Haeckel M, et al. Quantification of methane emissions at abandoned gas wells in the Central North Sea. *Mar Pet Geol.* 2015;68:848–60.
- Wang MY. Shallow natural gas in the modern Changjiang delta area. *Nat Gas Ind.* 1982;3:3–9 (in Chinese).
- Wang PX, Min QB, Bian YH, et al. Strata of Quaternary transgressions in east China: a preliminary study. *Acta Geol Sin.* 1981;55:1–13 (in Chinese).
- Wang PX, Zhang JJ, Zhao QH, et al. Foraminifera and Ostracod in Surface sediments of the East China Sea. Beijing: China Ocean Press; 1988. p. 1–438 (in Chinese).
- Wang ZH, Zhuang CC, Saito Y, et al. Early mid-Holocene sea-level change and coastal environmental response on the southern Yangtze delta plain, China: implications for the rise of Neolithic culture. *Quat Sci Rev.* 2012;35:51–62.
- Whiticar MJ, Faber E, Schoell M. Biogenic methane formation in marine and freshwater environments: CO<sub>2</sub> reduction vs. acetate fermentation-Isotope evidence. *Geochim Cosmochim Acta.* 1986;50(5):693–709.
- Whiticar MJ. Carbon and hydrogen isotope systematics of bacterial formation and oxidation of methane. *Chem Geol.* 1999;161(1–3):291–314.
- Wu M, Cao J, Wang XL, et al. Hydrocarbon generation potential of Triassic mudstones in the Junggar Basin, northwest China. *AAPG Bull.* 2014;98(9):1885–906.
- Xu ZY, Yue DL, Wu SH, et al. An analysis of the types and distribution characteristics of natural gas reservoirs in China. *Pet Sci.* 2009;6:38–42.
- Yang CS, Sun JS. Tidal sand ridges on the East China Sea shelf. In: de Boer PL, van Gelder A, Nio SD, editors. *Tide-influenced sedimentary environments and facies*. Dordrecht: D. Reidel Publ; 1988. p. 23–38.
- Yoneda M, Uno H, Shibata Y, et al. Radiocarbon marine reservoir ages in the western Pacific estimated by pre-bomb molluscan shells. *Nucl Instrum Methods Phys Res Sect B.* 2007;259(1):432–7.
- Zhang JQ, Zhang GJ, Li CX. Characteristics of the late Quaternary stratigraphic sequence in the Changjiang River delta area. *J Tongji Univ.* 1998;26(4):438–42 (in Chinese).
- Zhang X, Dalrymple RW, Yang SY, et al. Provenance of Holocene sediments in the outer part of the Paleo-Qiantang River estuary, China. *Mar Geol.* 2015;366(1):1–15.
- Zhang X, Lin CM, Dalrymple RW, et al. Facies architecture and depositional model of a macrotidal incised-valley succession (Qiantang River estuary, eastern China), and differences from other macrotidal systems. *GSA Bull.* 2014;126(3–4):499–522.

- Zhang X, Lin CM, Li YL, et al. Sealing mechanism for cap beds of shallow-biogenic gas reservoirs in the Qiantang River incised valley, China. *Cont Shelf Res.* 2013;69:155–67.
- Zhang YG, Chen HJ. Concepts on the generation and accumulation of biogenic gas. *Oil Gas Geol.* 1983;4(2):160–70 (**in Chinese**).
- Zheng KF. Distribution and exploration prospects of the shallow gas in the Quaternary in Jiangsu Province. *Nat Gas Ind.* 1998;18:20–4 (**in Chinese**).
- Zhou XJ, Gao S. Spatial variability and representation of seabed sediment grain sizes: an example from the Zhoushan-Jinshanwei transect, Hangzhou Bay, China. *Chin Sci Bull.* 2004;49(23):2503–7.
- Zhou ZH, Zhou RN, Guan ZQ. Geochemical properties of source materials and biogas prospects of the Quaternary gas in east of Qaidam basin. *Pet Explor Dev.* 1994;21:30–6 (**in Chinese**).
- Zhuang LH, Chang FM, Li TG, et al. Foraminiferal faunas and Holocene sedimentation rates of Core EY 02-2 in the South Yellow Sea. *Mar Geol Quatern Geol.* 2002;22:7–14 (**in Chinese**).
- Zou YR, Zhao CQ, Wang YP, et al. Characteristics and origin of natural gases in the Kuqa Depression of Tarim Basin, NW China. *Org Geochem.* 2006;37(3):280–90.